

We are IntechOpen, the world's leading publisher of Open Access books Built by scientists, for scientists

4,800

Open access books available

122,000

International authors and editors

135M

Downloads

Our authors are among the

154

Countries delivered to

TOP 1%

most cited scientists

12.2%

Contributors from top 500 universities



WEB OF SCIENCE™

Selection of our books indexed in the Book Citation Index
in Web of Science™ Core Collection (BKCI)

Interested in publishing with us?
Contact book.department@intechopen.com

Numbers displayed above are based on latest data collected.
For more information visit www.intechopen.com



Quantitative Dexterous Workspace Comparison of Serial and Parallel Planar Mechanisms

Geoff T. Pond and Juan A. Carretero
University of New Brunswick
Canada

1. Introduction

The dexterity analysis of complex degree of freedom (DOF) mechanisms has thus far been problematic. A well accepted method of measuring the dexterity of spherical or translational manipulators has been the Jacobian matrix condition number as in (Gosselin & Angeles, 1989) and (Badescu & Mavroidis, 2004). Unfortunately, the inconsistent units between elements within the Jacobian of a complex-DOF parallel manipulator do not allow such a measure to be generally made as discussed in (Tsai, 1999) and (Angeles, 2003). In the following section, the mathematical meaning of singular values and the condition number of a matrix are reviewed. Their application to studying robotic dexterity follows next. Later in this chapter, these principles are applied to the study and comparison of the dexterous workspace of both serial and parallel manipulators.

1.1 Mathematical background

The condition number of a matrix is defined as the ratio of the maximum and minimum singular values of the matrix. A brief explanation of the significance of the matrix's singular values is important and is therefore provided here. Strang (Strang, 2003) shows that any matrix or transform, *e.g.*, \mathbf{J} , may be broken into three components through singular value decomposition:

$$\mathbf{J} = \mathbf{U}\mathbf{\Sigma}\mathbf{V}^T \quad (1)$$

where \mathbf{V} contains the eigenvectors of $\mathbf{J}^T\mathbf{J}$, \mathbf{U} contains the eigenvectors of $\mathbf{J}\mathbf{J}^T$ (\mathbf{u}_1 and \mathbf{u}_2 for the two dimensional case shown) and $\mathbf{\Sigma}$ is a diagonal matrix containing the singular values of \mathbf{J} . Both the matrices \mathbf{V} and \mathbf{U} are composed of unit vectors which are mutually perpendicular within each matrix. Figure 1 is adapted from Strang (2003), and graphically depicts the transform described in equation (1) for the two dimensional case.

In terms of dexterity, the most interesting of the three component matrices of \mathbf{J} is $\mathbf{\Sigma}$ consisting of the singular values of \mathbf{J} each denoted by σ_i . Consider the conventional relation $\dot{\mathbf{q}} = \mathbf{J}\dot{\mathbf{x}}$, where in more general terms, $\dot{\mathbf{x}}$ corresponds to some unit system output depicted in the furthest left side of Figure 1, $\dot{\mathbf{q}}$, the system input depicted in the furthest right of Figure 1, and \mathbf{J} , the system transform between them. Generally, the maximum and

Source: Parallel Manipulators, New Developments, Book edited by: Jee-Hwan Ryu, ISBN 978-3-902613-20-2, pp. 498, April 2008, I-Tech Education and Publishing, Vienna, Austria

minimum singular values of J indicate a range within which the magnitude of vector \dot{q} must lie, for any unit output in \dot{x} , i.e., $|\dot{x}| = 1$. The condition number κ is then the ratio of the largest and smallest singular values:

$$\kappa = \frac{\sigma_{max}}{\sigma_{min}} \quad (2)$$

The diagram illustrates the three steps in any matrix transformation: rotation, scaling, and rotation (or reflection). It shows a sequence of four coordinate systems. The first shows a unit circle with axes v_1 and v_2 , and a vector V . The second shows a unit circle with axes σ_1 and σ_2 . The third shows an ellipse with axes σ_1 and σ_2 . The fourth shows an ellipse with axes $\sigma_1 u_1$ and $\sigma_2 u_2$. Arrows labeled V^T , Σ , and U indicate the transformations between the steps.

Figure 1: The three steps in any matrix transformation: rotation, scaling, rotation (or reflection).

Now, let the system output \dot{x} correspond to the velocity vector of a manipulator's end effector and \dot{q} , the vector of actuator velocities. 'Ideal dexterity' occurs at isotropic conditions, that is at the lowest possible Jacobian condition number, i.e., 1 (Angeles, 2003). At such positions, a unit velocity in any feasible direction for the manipulator requires the same total effort in the actuators, i.e., the resolution of end effector pose is the same in each DOF. On the other hand, a condition number of ∞ corresponds to a rank deficiency within the Jacobian matrix. At such configurations, some level of control over the system is lost.

1.2 Application to robotics

In robotics, the Jacobian, and hence its singular values and condition number, are dependant on the architecture of the manipulator as well as the position and orientation, together referred to as pose, of the manipulator's end effector. As a result, the manipulator's level of dexterity changes as it travels through its reachable workspace. A manipulator's dextrous workspace is often defined as poses resulting in a Jacobian matrix condition number below a specified threshold. The higher level of dexterity required, or as conventionally defined, the lower the condition number, the smaller the dextrous workspace will be. This is due to an increasing Jacobian matrix condition number as the reachable workspace boundary is approached. Manipulator singularities exist when the Jacobian condition number becomes infinite, that is, either a) an instantaneously infinite actuator input velocity results in no change in the end effector pose, or b) the end effector pose may be altered without having changed the actuator inputs.

However, using the Jacobian condition number alone may provide misleading results, particularly when comparing multiple manipulators, as this chapter will later do. Consider two 2-DOF manipulators, of the same architecture but of different scale, and in the same pose. The first having Jacobian matrix singular values of 1 and 2, the second being 100 times larger having singular values of 100 and 200. Both result in the same condition number as they both require twice the effort in the second direction as they do to move in the first. That is, the magnitude of the vector $\dot{\mathbf{q}}$ required to perform the motion in the second direction is twice as large in magnitude as the magnitude required to perform the motion in the first direction. In the case of the first system, the end effector pose is far more sensitive to the system inputs (recall that the sensitivity is indicated by the singular values, the condition number only indicates the ratio of this sensitivity for the fastest and slowest directions in the task space). For this reason, the entries of the Jacobian matrix must all share the same units, *e.g.*, distances may be measured in *m* but not by a mix of *m*, *cm*, *mm*, *etc.*

Larger singular values correspond to a better resolution over the pose of the end effector, hence better position control over the mechanism end effector pose is achieved. However, having small singular values also has a benefit. Having smaller singular values suggests that the same system outputs are achieved at lower system inputs when compared to a system with large singular values. This corresponds to higher end effector velocities for the same actuator input magnitude. Therefore, there is a trade-off between high end effector velocities (a Jacobian having small singular values), and fine resolution over the end effector pose which provides better stiffness and accuracy (a Jacobian having large singular values).

In terms of dexterity, higher end effector velocities are generally of greater concern. In terms of either accuracy or stiffness / compliance, a finer resolution over the end effector pose is of greater importance. Therefore, examination of the Jacobian matrix condition number alone, does not fully describe the capabilities of a manipulator in the studied pose.

1.3 Issues with using the Jacobian matrix condition number

It is well known that the use of the condition number of a manipulator's Jacobian matrix to measure dexterity may only be made when all the entries that constitute such a Jacobian matrix share the same units (Tsai, 1999; Angeles, 2003; Doty et al., 1995). This limits the use of the Jacobian condition number to manipulators that have only one type of actuator (*i.e.*, either revolute or prismatic, but not a combination of both). Furthermore, use of the Jacobian condition number is restricted to manipulators having only degrees of freedom (DOF) in either Cartesian or rotational directions only, but not combinations of both. The only mechanisms that fall into this category are 3-DOF (or less) rotational and 3-DOF (or less) translational manipulators. Otherwise, if the manipulator has a mix of revolute and prismatic actuators, or has complex degrees of freedom, their associated Jacobian matrix is dimensionally inconsistent.

As stated earlier, the Jacobian condition number has been a popular measure of dexterity in many works for either of these types of rotational or translational mechanisms (Gosselin & Angeles, 1989; Tsai & Joshi, 2000; Badescu & Mavroidis, 2004). For manipulators outside of this category, the condition number of conventional Jacobian matrices developed by methods such as screw theory or by partial derivatives, is not suitable for dexterity measurement due to their inherent mixture of units between the different columns of \mathbf{J} (Tsai, 1999; Angeles, 2003; Doty et al., 1995). This leaves no method for the general algebraic formulation of dimensionally homogeneous Jacobian matrices. Therefore, no method is left

for reliably measuring or quantifying the dexterity of a vast majority of mechanisms introduced in the literature that have mobility in both translational and rotational DOF, *i.e.*, complex DOF mechanisms (*e.g.*, Stewart, 1965; Lee & Shah, 1988; Siciliano, 1999; Carretero et al., 2000).

Gosselin (1992) introduced a method for formulating a dimensionally-homogeneous Jacobian matrix for both planar and some spatial mechanisms. Planar mechanisms have two translational and one rotational DOF. For the planar case, this Jacobian matrix relates the actuator velocities to the x and y components of the velocities of two points on the end effector platform. Kim and Ryu (2003) furthered this work by developing a general method using the x , y and z velocity components of three points (as opposed to two in (Gosselin, 1992)) on the end effector platform (A_1 , A_2 and A_3) to formulate a Jacobian matrix which maps m actuator velocities (where m denotes the number of actuators) to the nine Cartesian velocity components of the three points A_i (*i.e.*, three for each point A_i). Assuming all actuators are of the same type, this $m \times 9$ Jacobian is dimensionally-homogeneous, regardless of the conventionally defined independent end effector variables (*i.e.*, translational and/or angular velocities). However, of the total nine x , y and z velocity components (three for each point), at most only n are independent for a mechanism whose task space is n -DOF, where $n \leq 6$. This suggests that $(9 - n)$ terms of the end effector velocity vector may be defined as dependent variables. As this velocity vector and therefore the associated Jacobian includes dependent motions, it is not evident what physical significance the singular values of such a Jacobian matrix might have (Kim & Ryu, 2003). Therefore, using the ratio of maximum and minimum singular values (*i.e.*, the condition number) of the Jacobian matrix seems ill-advised.

In (Pond & Carretero, 2006), the authors present a methodology for obtaining a constrained and dimensionally homogeneous Jacobian based on an extension of the work in (Kim & Ryu, 2003). The singular values of such Jacobians may be used in dexterity analyses as their physical interpretation is typically clear. In the following section, the development of this type of Jacobian matrix is presented for the 3-RRR planar parallel manipulator.

2. The 3-RRR planar parallel manipulator

The symmetrical 3-RRR manipulator depicted in Figure 2 has been the subject of many studies. For example, inverse kinematics including velocity and acceleration, as well as singularity analysis, are provided by (Gosselin, 1988). It is a relatively simple, planar parallel manipulator, as described in the following section.

2.1 Mechanism architecture

As seen in Figure 2, the symmetrical 3-RRR manipulator consists of three identical limbs. Each limb is connected to the base at point G_i by an actuated revolute joint. This is followed by a *proximal* link of length $|\mathbf{b}_i|$ which connects to the *distal* link of length $|\mathbf{c}_i|$ through a passive revolute joint at B_i . Finally, a second passive revolute joint connects each limb to the end effector platform at point A_i . For the symmetric case, points G_i and A_i may each be used to form the corners of equilateral triangles.

For the planar 3-RRR manipulator, all joint axes are parallel and normal to the xy -plane. It can be easily demonstrated using the Grübler-Kutzbach mobility criterion that the mobility of the 3-RRR equals 3.

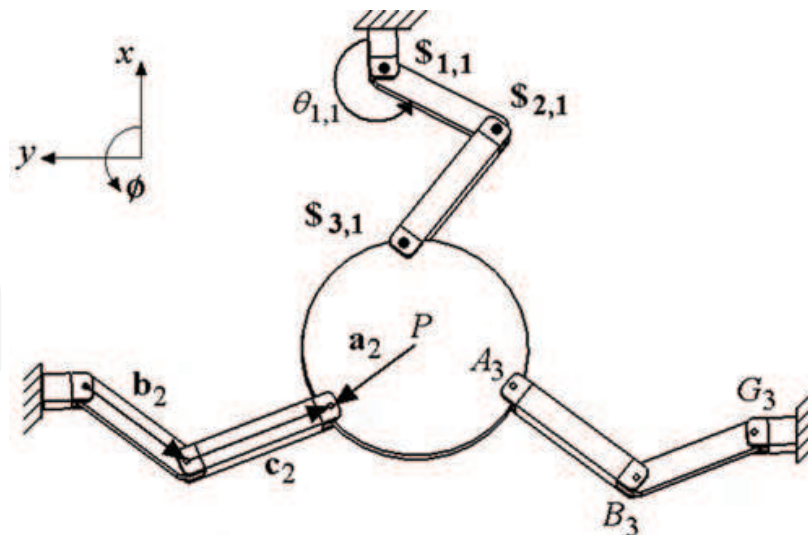


Figure 2: Basic architecture of the 3-RRR parallel manipulator.

The degrees of freedom at the end effector are translations in the x and y directions and a rotation ϕ , around an axis normal to the xy -plane. Note that the base frame's origin is placed coincident with the centre of a circle intersecting each of the three points G_i located at the base of each branch. The x -axis of the base frame is oriented such that point G_1 lies on that axis.

As the inverse displacement solution of this manipulator are previously published, no further discussion on the subject will be provided here. The Jacobian formulation provided for this manipulator in (Gosselin, 1988) and (Arsenault & Boudreau, 2004) is developed by differentiating the various inverse displacement equations, with respect to time. In (Tsai, 1999), the Jacobian matrix was obtained through the method of cross-products. In what follows, the conventional inverse and direct Jacobian matrices will instead, be obtained through screw theory.

2.2 Jacobian analysis using screw theory

The Jacobian developed here will relate the Cartesian velocities of the end effector in \dot{x} , \dot{y} and $\dot{\phi}$ (or ω_z in conventional screw coordinate notation) to the actuator velocities.

Three screws $\$_{1,i}$, $\$_{2,i}$ and $\$_{3,i}$, with directions normal to the xy -plane, represent the three joints of each limb i for $i = 1, 2, 3$ (depicted in Figure 2 for $i = 1$):

$$\$_{1,i} = \begin{bmatrix} \mathbf{s}_{1,i} \\ (\mathbf{a}_i - \mathbf{c}_i - \mathbf{b}_i) \times \mathbf{s}_{1,i} \end{bmatrix} \quad (3)$$

$$\$_{2,i} = \begin{bmatrix} \mathbf{s}_{2,i} \\ (\mathbf{a}_i - \mathbf{c}_i) \times \mathbf{s}_{2,i} \end{bmatrix} \quad (4)$$

$$\mathcal{S}_{3,i} = \begin{bmatrix} \mathbf{s}_{3,i} \\ \mathbf{a}_i \times \mathbf{s}_{3,i} \end{bmatrix} \quad (5)$$

Each screw is represented with respect to a frame whose origin is coincident with that of the moving frame, *i.e.*, at point P , but whose axes are parallel to those of the fixed frame. The direction of all screws ($\mathbf{s}_{j,i}$) is the same for all of them as all are aligned with the z -axis. Therefore, the screw corresponding to the platform's motion is:

$$\mathcal{S}_p = \dot{\theta}_{1,i} \mathcal{S}_{1,i} + \dot{\theta}_{2,i} \mathcal{S}_{2,i} + \dot{\theta}_{3,i} \mathcal{S}_{3,i} \quad (6)$$

where angle $\theta_{j,i}$ corresponds to the rotation around the j -th revolute joint ($j = 1, 2, 3$) of the i -th limb ($i = 1, 2, 3$).

A screw must now be identified that is reciprocal to all screws representing the passive joints of limb i , *i.e.*, the revolute joints at points A_i and B_i . Such a screw may be zero pitch and oriented anywhere on the plane containing vectors \mathbf{c}_i and $\mathbf{s}_{2,i}$ (or $\mathbf{s}_{3,i}$ corresponding to screws $\mathcal{S}_{2,i}$ and $\mathcal{S}_{3,i}$ in Figure 2). Such a reciprocal screw is:

$$\mathcal{S}_{r,i} = \begin{bmatrix} \mathbf{s}_{r,i} \\ \mathbf{a}_i \times \mathbf{s}_{r,i} \end{bmatrix} = \begin{bmatrix} \hat{\mathbf{c}}_i \\ \mathbf{a}_i \times \hat{\mathbf{c}}_i \end{bmatrix} = \frac{1}{|\mathbf{c}_i|} \begin{bmatrix} \mathbf{c}_i \\ \mathbf{a}_i \times \mathbf{c}_i \end{bmatrix} \quad (7)$$

$$= \frac{1}{|\mathbf{c}_i|} \begin{bmatrix} c_{ix} & c_{iy} & 0 & 0 & 0 & a_{ix}c_{iy} - a_{iy}c_{ix} \end{bmatrix}^T \quad (8)$$

where $\hat{\mathbf{c}}_i$ is a unit vector in the direction of \mathbf{c}_i . Taking the orthogonal product (here denoted by \otimes) of $\mathcal{S}_{r,i}$ with both sides of equation (6), yields:

$$\mathcal{S}_{r,i} \otimes \mathcal{S}_p = \mathcal{S}_{r,i} \otimes \mathcal{S}_{1,i} \dot{\theta}_{1,i} \quad (9)$$

where $\mathcal{S}_p = [\omega_x \ \omega_y \ \omega_z \ \dot{x} \ \dot{y} \ \dot{z}]^T$. Since an orthogonal product involving screw $\mathcal{S}_{r,i}$ is on both sides of equation (9), the coefficient $1/|\mathbf{c}_i|$ shown in equation (8) may be dropped. To simplify notation, recognising that $\omega_x = \omega_y = \dot{z} = 0$ (since motion only occurs on xy -plane), $\mathcal{S}_{r,i}$ and \mathcal{S}_p may be reduced to three dimensional vectors, *i.e.*, $\mathcal{S}_{r,i} = [c_{ix} \ c_{iy} \ (a_{ix}c_{iy} - a_{iy}c_{ix})]^T$ and $\mathcal{S}_p = [\omega_z \ \dot{x} \ \dot{y}]^T$.

Examining the right side of equation (9), and reducing $\mathcal{S}_{1,i}$ in equation (3), the orthogonal product $\mathcal{S}_{r,i} \otimes \mathcal{S}_{1,i}$ may be expressed as:

$$\mathcal{S}_{r,i} \otimes \mathcal{S}_{1,i} = \begin{bmatrix} (a_{ix}c_{iy} - a_{iy}c_{ix}) & c_{ix} & c_{iy} \end{bmatrix} \begin{bmatrix} 1 \\ (a_i - c_i - b_i)_y \\ -(a_i - c_i - b_i)_x \end{bmatrix} = b_{ix}c_{iy} - b_{iy}c_{ix} \quad (10)$$

Therefore, writing equation (9) three times corresponding to each of the mechanism's limbs yields the following direct (\mathbf{J}_x) and inverse (\mathbf{J}_q) Jacobians expressed as:

$$\mathbf{J}_x = \begin{bmatrix} a_{1x}c_{1y} - a_{1y}c_{1x} & c_{ix} & c_{iy} \\ a_{2x}c_{2y} - a_{2y}c_{2x} & c_{ix} & c_{iy} \\ a_{3x}c_{3y} - a_{3y}c_{3x} & c_{ix} & c_{iy} \end{bmatrix}_{3 \times 3} \quad (11)$$

$$\mathbf{J}_q = \begin{bmatrix} b_{1x}c_{1y} - b_{1y}c_{1x} & 0 & 0 \\ 0 & b_{2x}c_{2y} - b_{2y}c_{2x} & 0 \\ 0 & 0 & b_{3x}c_{3y} - b_{3y}c_{3x} \end{bmatrix}_{3 \times 3} \quad (12)$$

The results of \mathbf{J}_x and \mathbf{J}_q correspond exactly with those obtained by (Tsai, 1999) through the cross product method and by (Arsenault & Boudreau, 2004) through calculus. The resulting overall Jacobian matrix $\mathbf{J} = \mathbf{J}_q^{-1}\mathbf{J}_x$ is a square 3×3 matrix. The relation between end effector and actuator velocities is $\dot{\mathbf{q}} = \mathbf{J}\dot{\mathbf{x}}$ where $\dot{\mathbf{q}} = [\dot{\theta}_{1,1} \ \dot{\theta}_{1,2} \ \dot{\theta}_{1,2}]^T$ and $\dot{\mathbf{x}} = [\omega_z \ \dot{x} \ \dot{y}]^T$.

In the following section, the Jacobian matrix \mathbf{J} will be used as a verification tool to evaluate whether the Jacobian matrices formulated the more novel introduced in (Pond & Carretero, 2006) methods are correct.

2.3 Constrained dimensionally-homogeneous Jacobian matrix formulation

As mentioned, the Jacobian matrix \mathbf{J} developed in the previous section is dimensionally inconsistent. In (Tsai, 1999) and (Angeles, 2003), the authors have outlined the importance in having a dimensionally-homogeneous Jacobian matrix in dexterity analyses.

In (Kim & Ryu, 2003), the following velocity relation was developed:

$$\dot{\mathbf{q}} = (\mathbf{J}'_q)^{-1}\mathbf{J}'_x\dot{\mathbf{x}}' \quad (13)$$

Where, letting $\bar{\mathbf{k}} = [0 \ 0 \ 1]^T$, $\dot{\mathbf{q}} = [\dot{\theta}_{1,1} \ \dot{\theta}_{1,2} \ \dot{\theta}_{1,2}]^T$ and $\dot{\mathbf{x}}' = [\dot{A}_{1x} \ \dot{A}_{1y} \ \dot{A}_{2x} \ \dot{A}_{2y} \ \dot{A}_{3x} \ \dot{A}_{3y}]^T$:

$$\mathbf{J}'_q = \begin{bmatrix} \mathbf{c}_1^T (\bar{\mathbf{k}} \times \mathbf{b}_1) & 0 & 0 \\ 0 & \mathbf{c}_2^T (\bar{\mathbf{k}} \times \mathbf{b}_2) & 0 \\ 0 & 0 & \mathbf{c}_3^T (\bar{\mathbf{k}} \times \mathbf{b}_3) \end{bmatrix}_{3 \times 3} \quad (14)$$

$$\mathbf{J}'_x = \begin{bmatrix} k_{1,1}\mathbf{c}_1^T & k_{1,2}\mathbf{c}_1^T & k_{1,3}\mathbf{c}_1^T \\ k_{2,1}\mathbf{c}_2^T & k_{2,2}\mathbf{c}_2^T & k_{2,3}\mathbf{c}_2^T \\ k_{3,1}\mathbf{c}_3^T & k_{3,2}\mathbf{c}_3^T & k_{3,3}\mathbf{c}_3^T \end{bmatrix}_{3 \times 6} \quad (15)$$

Parameters $k_{i,j}$ (for $i = 1, 2, 3$ and $j = 1, 2, 3$) are dimensionless parameters defining the parametric equation of a plane containing the three points on the end effector platform and constrained by $k_{i,1} + k_{i,2} + k_{i,3} = 1$. It can be shown (Pond, 2006) that when using the Jacobian formulation as presented in this section, $k_{i,j} = 1$ when $i = j$ and $k_{i,j} = 0$ otherwise.

The multiplication of $(J'_q)^{-1}J'_x$ using the dimensionally homogeneous Jacobian matrices above produces the overall Jacobian matrix J' which is equivalent to:

$$J' = \begin{bmatrix} \frac{\partial \theta_{1,1}}{\partial A_{1x}} & \frac{\partial \theta_{1,1}}{\partial A_{1y}} & \frac{\partial \theta_{1,1}}{\partial A_{2x}} & \frac{\partial \theta_{1,1}}{\partial A_{2y}} & \frac{\partial \theta_{1,1}}{\partial A_{3x}} & \frac{\partial \theta_{1,1}}{\partial A_{3y}} \\ \frac{\partial \theta_{1,2}}{\partial A_{1x}} & \frac{\partial \theta_{1,2}}{\partial A_{1y}} & \frac{\partial \theta_{1,2}}{\partial A_{2x}} & \frac{\partial \theta_{1,2}}{\partial A_{2y}} & \frac{\partial \theta_{1,2}}{\partial A_{3x}} & \frac{\partial \theta_{1,2}}{\partial A_{3y}} \\ \frac{\partial \theta_{1,3}}{\partial A_{1x}} & \frac{\partial \theta_{1,3}}{\partial A_{1y}} & \frac{\partial \theta_{1,3}}{\partial A_{2x}} & \frac{\partial \theta_{1,3}}{\partial A_{2y}} & \frac{\partial \theta_{1,3}}{\partial A_{3x}} & \frac{\partial \theta_{1,3}}{\partial A_{3y}} \end{bmatrix} \quad (16)$$

It is important to only map a set of independent end effector velocities to the actuator velocities. The mapping being done in equation (13) maps six end effector velocities of which only three are independent (for the 3-DOF mechanism) to the three actuator velocities. Similar to what is presented in (Pond & Carretero, 2006), a constraining matrix mapping the independent end effector velocities to the full set of both independent and dependent end effector velocities may be obtained.

If a constraining matrix P that maps the Cartesian velocities $\dot{A}_{1x}, \dot{A}_{2x}, \dot{A}_{3y}$, to all velocities in \dot{x}' was obtainable, it could be expressed in terms of partial derivatives, as follows:

$$P = \begin{bmatrix} 1 & \frac{\partial A_{1y}}{\partial A_{1x}} & 0 & \frac{\partial A_{2y}}{\partial A_{1x}} & \frac{\partial A_{3x}}{\partial A_{1x}} & 0 \\ 0 & \frac{\partial A_{1y}}{\partial A_{2x}} & 1 & \frac{\partial A_{2y}}{\partial A_{2x}} & \frac{\partial A_{3x}}{\partial A_{2x}} & 0 \\ 0 & \frac{\partial A_{1y}}{\partial A_{3y}} & 0 & \frac{\partial A_{2y}}{\partial A_{3y}} & \frac{\partial A_{3x}}{\partial A_{3y}} & 1 \end{bmatrix}^T \quad (17)$$

The resulting multiplication of J' in equation (16) with the constraining matrix P in equation (17) yields:

$$J'P = \begin{bmatrix} \frac{\partial \theta_{1,1}}{\partial A_{1x}} & \frac{\partial \theta_{1,1}}{\partial A_{2x}} & \frac{\partial \theta_{1,1}}{\partial A_{3y}} \\ \frac{\partial \theta_{1,2}}{\partial A_{1x}} & \frac{\partial \theta_{1,2}}{\partial A_{2x}} & \frac{\partial \theta_{1,2}}{\partial A_{3y}} \\ \frac{\partial \theta_{1,3}}{\partial A_{1x}} & \frac{\partial \theta_{1,3}}{\partial A_{2x}} & \frac{\partial \theta_{1,3}}{\partial A_{3y}} \end{bmatrix} \quad (18)$$

This matrix $J'P$ is square and dimensionally homogeneous. The singular values of this matrix have a clear physical interpretation and therefore may be used in the dexterity analysis of the corresponding mechanism.

2.3.1 Identification of independent parameters

To obtain equation (18), the set $\dot{A}_{1x}, \dot{A}_{2x}, \dot{A}_{3y}$ was chosen as the set of independent Cartesian components. Clearly, six unique sets of independent parameters may be used to define the end effector velocity \dot{x}'' . That is, any subset consisting of three elements from the six elements of \dot{x}' which includes at least one x component and at least one y component may be used. These subsets are:

Case I:	$[\dot{A}_{1x} \ \dot{A}_{2x} \ \dot{A}_{3y}]^T$	Case IV:	$[\dot{A}_{1y} \ \dot{A}_{2y} \ \dot{A}_{3x}]^T$
Case II:	$[\dot{A}_{1x} \ \dot{A}_{2y} \ \dot{A}_{3x}]^T$	Case V:	$[\dot{A}_{1y} \ \dot{A}_{2x} \ \dot{A}_{3y}]^T$
Case III:	$[\dot{A}_{1y} \ \dot{A}_{2x} \ \dot{A}_{3x}]^T$	Case VI:	$[\dot{A}_{1x} \ \dot{A}_{2y} \ \dot{A}_{3y}]^T$

In the following formulation of the constraint equations and alternative inverse displacement solution, the independent end effector parameters will be arbitrarily chosen as Case I (*i.e.*, $\dot{A}_{1x}, \dot{A}_{2x}, \dot{A}_{3y}$). The solutions using any of the potential six cases listed above have a similar form.

2.3.2 Constraint equations

It can in fact be shown that a relationship between $[\dot{A}_{1x}, \dot{A}_{2x}, \dot{A}_{3y}]^T$ to $\dot{\mathbf{x}}$, *i.e.*, the matrix **P** in equation (18), can be obtained. Consider Figure 3 representing the end effector platform. The point *D* lies on the bisection of the line segment A_1A_2 so:

$$D_x = A_{1x} + (A_{2x} - A_{1x})/2$$

(19)

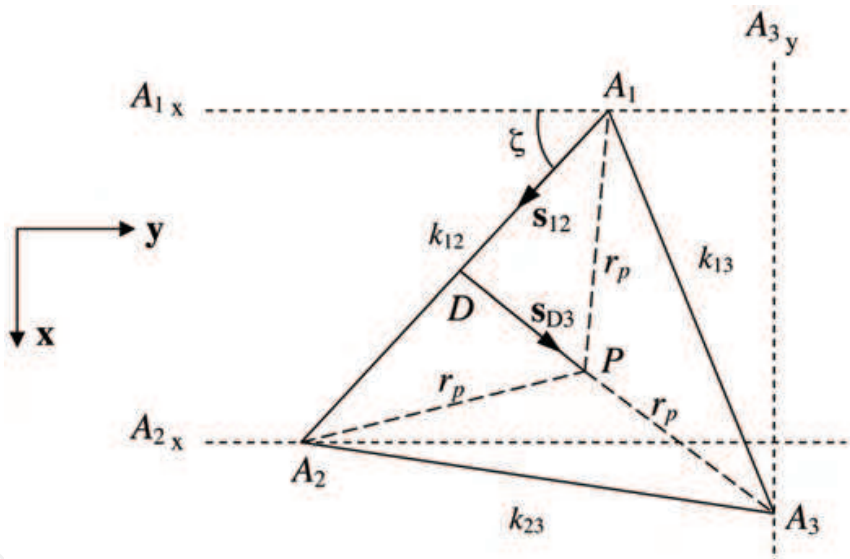


Figure 3: End effector notation for the planar 3-RRR parallel manipulator. The angle ζ made between line segment A_1A_2 with the negative y -axis is:

$$\zeta = \sin^{-1} \left(\frac{|A_{2x} - A_{1x}|}{k_{12}} \right)$$

(20)

where k_{12} is the length of the line segment between points A_1 and A_2 . Consider the case where the variables A_{1x} , A_{2x} and A_{3y} are known. Therefore, the vertices of the triangle representing the end effector platform lie somewhere on the three dashed lines shown in Figure 3. When these three dashed lines are used to constrain the vertices of the end effector platform, there are two possible solutions for the unit vector s_{12} :

$$\mathbf{s}_{12} = [s_\zeta \quad \pm c_\zeta \quad 0]^T \quad (21)$$

The vector \mathbf{s}_{D3} may be obtained by cross multiplying the vector \mathbf{s}_{12} with $\pm \bar{\mathbf{k}}$ (recalling that $\bar{\mathbf{k}} = [0 \ 0 \ 1]^T$):

$$\mathbf{s}_{D3} = \mathbf{s}_{12} \times \pm \bar{\mathbf{k}} = [\pm c_\zeta \quad \pm s_\zeta \quad 0]^T \quad (22)$$

As a result, there are four possible solutions for vector \mathbf{s}_{D3} each corresponding to one of the four unique solutions in Figure 4.

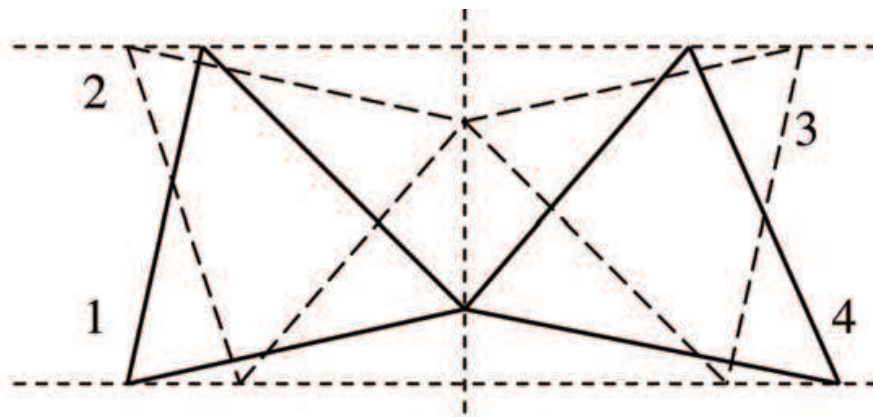


Figure 4: Four possible solutions where a single Cartesian coordinate of each of three points on the end effector platform are known.

Letting e represent the magnitude of the line segment \overline{DP} :

$$e = \sqrt{\left(r_p^2 - \frac{k_{12}^2}{4}\right)} \quad (23)$$

where k_{12} can be obtained from the platform radius r_p and the angle between lines $\overline{PA_1}$ and $\overline{PA_2}$. Letting vector \mathbf{D} represent a vector from the origin of the base frame to point D (see Figure 3), a solution for the vector \mathbf{A}_3 locating point A_3 with respect to the origin is:

$$\mathbf{A}_3 = \mathbf{D} + (e + r_p) [\pm c_\zeta \quad \pm s_\zeta \quad 0]^T \quad (24)$$

From which the first component is

$$A_{3x} = D_x \pm (e + r_p) c_\zeta \quad (25)$$

The same method may then be reversed to find $D_y = A_{3y} \pm (e + r_p) s_\zeta$. Similarly, solutions are found for A_{1y} and A_{2y} as:

$$A_{1y} = D_y + \left(\frac{k_{12}}{2}\right)(\pm c_\zeta) \quad (26)$$

$$A_{2y} = D_y - \left(\frac{k_{12}}{2}\right)(\pm c_\zeta) \quad (27)$$

To obtain a single solution for the direction of vector s_{D3} instead of the four possible solutions in equation (22), the true position and orientation of the platform in conventional variables, *i.e.*, x , y and ϕ , are required. Since in workspace volume determination or path planning, these are in fact known, the following decision rules may be used to obtain a unique solution in the coordinates A_{1x} , A_{1y} , A_{2x} , A_{2y} , A_{3x} and A_{3y} . If $x > D_x$, then all terms associated with $\pm c_\zeta$ are in fact $+c_\zeta$ and vice versa. Similarly, if $A_{3y} > y$, then all terms associated with $\pm s_\zeta$ are in fact $+s_\zeta$ and vice versa.

2.3.3 Alternative inverse displacement solution

In the preceding section, the remaining three Cartesian coordinates of the three points A_i were determined based on one of the Cartesian coordinates being given for each point. This provides full knowledge as to the position of the end effector platform and points A_i . The solution for each limb's pose may be obtained by completing the inverse displacement solution provided in (Tsai, 1999) or (Arsenault & Boudreau, 2004) where points A_i are known. The solution leads to two solutions for each limb. In (Arsenault & Boudreau, 2004), these are referred to as *working modes*. The different solutions correspond to either *elbow up* or *elbow down* configurations of each limb. As there are two solutions for each limb, and three limbs, there are therefore a total of $2^3 = 8$ possible solutions to the inverse displacement problem.

2.3.4 Constraining Jacobian

The first derivative with respect to time of equations (25) through (27) yields the various elements of the matrix \mathbf{P} in equation (17). As previously mentioned, six unique sets of independent end effector variables may be used to obtain the square dimensionally-homogeneous Jacobian matrix.

2.4 Singularity analysis

Singularity analysis of the 3-RRR manipulator has been explored extensively in (Tsai, 1999; Bonev & Gosselin, 2001; Arsenault & Boudreau, 2004). Essentially two singularities exist for this manipulator. An inverse singular configuration occurs whenever one of the three limbs is fully stretched out, or when the distal link overlaps the proximal link of any limb. At such configurations, instantaneous rotations of the actuated revolute joint do not alter the end effector pose.

A direct singular configuration exists whenever the lines collinear with the distal links have a common intersection for all three limbs. In Figure 2, the direction of these lines is represented for limb 2 by vector \mathbf{c}_2 . At these singular configurations, an instantaneous

rotation around the point of intersection of the above mentioned lines, may be obtained without any displacement of the actuators.

Singular configurations are also mathematically introduced by the constraining matrix **P** which do not correspond to physical singular configurations of the manipulator. First, recall the equilateral triangle $A_1A_2A_3$ used to model the end effector (Figure 5). The mechanism’s degrees of freedom include a translational ability in x and y and a rotational ability in the plane, *i.e.*, angle ϕ . These three points were used in the formulation of the 3×6 dimensionally homogeneous Jacobian matrix **J**’.

For each of the six sets of potential independent end effector variables for the planar mechanisms described in Section 2.3.1, the poses listed in Table 1 are observed to yield a rank deficient constrained and dimensionally homogeneous Jacobian matrix **J****P**.

It is also observed that these singular configurations occur at all x and y positions tested. For the first three cases, where two of the three x -coordinates are considered independent, these singular configurations are introduced when the line made between the two points, whose x -coordinates are independent, is parallel with the x -axis. Similarly, for the last three cases where two of the three y coordinates are considered independent, these singular configurations occur when the line made between the two points, whose y -coordinates are independent, is parallel with the y -axis.

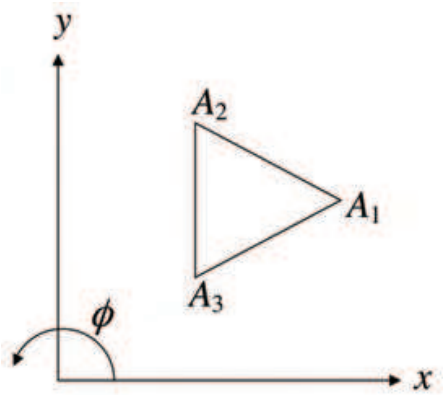


Figure 5: The end effector of a planar mechanism modelled as a triangle. End effector is at a mathematically-introduced singularity if independent variables in Case VI are chosen.

Case No.	Independent Parameters	Mathematically Singular Poses
I	$[\dot{A}_{1x} \ \dot{A}_{2x} \ \dot{A}_{3y}]^T$	$\phi = 30^\circ, 210^\circ, -150^\circ, -330^\circ$
II	$[\dot{A}_{1x} \ \dot{A}_{2y} \ \dot{A}_{3x}]^T$	$\phi = -30^\circ, -210^\circ, 150^\circ, 330^\circ$
III	$[\dot{A}_{1y} \ \dot{A}_{2x} \ \dot{A}_{3x}]^T$	$\phi = 90^\circ, 270^\circ, -90^\circ, -270^\circ$
IV	$[\dot{A}_{1y} \ \dot{A}_{2y} \ \dot{A}_{3x}]^T$	$\phi = -60^\circ, -240^\circ, 120^\circ, 300^\circ$
V	$[\dot{A}_{1y} \ \dot{A}_{2x} \ \dot{A}_{3y}]^T$	$\phi = 60^\circ, 240^\circ, -120^\circ, -300^\circ$
VI	$[\dot{A}_{1x} \ \dot{A}_{2y} \ \dot{A}_{3y}]^T$	$\phi = 0^\circ, 180^\circ, -180^\circ$

Table 1: Observed mathematically-introduced singularities for the 3-RRR planar parallel manipulator.

The source of this issue is a function of the constraints being imposed by the manipulator’s limbs.

The points A_1 , A_2 and A_3 are constrained to lie in the xy -plane. Recall that the constraining matrix \mathbf{P} is formulated based on the implicit constraints imposed on the end effector by the manipulator's limbs, but not explicitly on the architecture itself.

The following is a purely mathematical examination of the terms within the constraining matrix \mathbf{P} which create the rank deficiencies not inherent to the mechanism.

Consider Case VI as listed in Section 2.3.1, where the independent parameters are identified as A_{1x} , A_{2y} and A_{3y} . The following is a symbolic representation of the resulting constraint matrix:

$$\mathbf{P}_6 = \begin{bmatrix} 1 & 0 & 0 \\ \frac{\partial A_{1y}}{\partial A_{1x}} & \frac{\partial A_{1y}}{\partial A_{2y}} & \frac{\partial A_{1y}}{\partial A_{3y}} \\ \frac{\partial A_{2x}}{\partial A_{1x}} & \frac{\partial A_{2x}}{\partial A_{2y}} & \frac{\partial A_{2x}}{\partial A_{3y}} \\ 0 & 1 & 0 \\ \frac{\partial A_{3x}}{\partial A_{1x}} & \frac{\partial A_{3x}}{\partial A_{2y}} & \frac{\partial A_{3x}}{\partial A_{3y}} \\ 0 & 0 & 1 \end{bmatrix} \quad (28)$$

Given the independent parameters associated with Case VI, the equivalent angle ζ of Figure 3 is defined as:

$$\zeta = \sin^{-1} \left(\frac{|A_{3y} - A_{2y}|}{k_{23}} \right) \quad (29)$$

where k_{23} is the length of the line segment between points A_2 and A_3 . The angle ζ is defined differently depending on the identified independent parameters. The partial derivative $\partial\zeta$ taken with respect to the various independent parameters, appears in the formulation of many of the entries of equation (28). As a result, when the line between points A_2 and A_3 is parallel with the y -axis (as depicted in Figure 5), the magnitude of the projection of line segment (A_2A_3) onto the y -axis will instantaneously undergo no change for any change in angle ζ . Therefore, the partial derivative $\partial\zeta / \partial|A_{3y} - A_{2y}|$ is equal to infinity. For instance, for a pose where $\phi = 0^\circ$, the constraining matrix \mathbf{P} may be expressed numerically as:

$$\mathbf{P}_6 = \begin{bmatrix} 1 & 0 & 0 \\ 0 & \infty & -\infty \\ 1 & -\infty & \infty \\ 0 & 1 & 0 \\ 1 & 0 & 0 \\ 0 & 0 & 1 \end{bmatrix} \quad (30)$$

As discussed, Jacobian matrices obtained for the other five cases at the same pose, are not rank deficient and therefore may still be used to obtain a measurement of dexterity.

3. Dexterity measurement

One of the objectives of performing dexterity analyses on parallel manipulators is to obtain an understanding of how sensitive the end effector pose is relative to the actuator displacement. As discussed, for some cases, this has historically been achieved through observation of the Jacobian matrix condition number.

The condition number of the screw based Jacobian matrix \mathbf{J} and dimensionally homogeneous Jacobian matrix \mathbf{J}' throughout a chosen path are depicted in Figure 6. Clearly, the planned trajectory either passes through or very near a singular configuration as evidenced by the rapidly increasing condition number of the screw-based Jacobian matrix at approximately $t = 0.9$ sec. In fact, it can be shown that for the defined path, the manipulator passes through a direct singular configuration where the three vectors \mathbf{c}_i depicted in Figure 2 intersect at a single point.

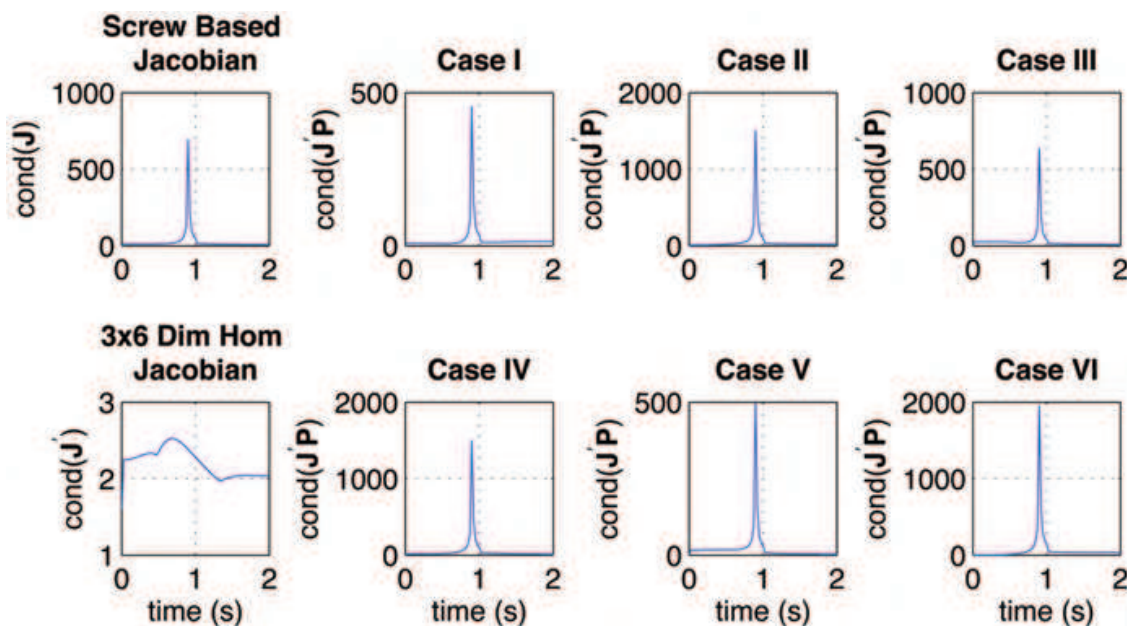


Figure 6: The condition number of each of the formulated Jacobian matrices throughout the planned trajectory.

However, \mathbf{J}' , the 3×6 dimensionally homogeneous Jacobian matrix developed by (Kim & Ryu, 2003), does not suggest the same. Instead, its condition number gives the impression that the manipulator is relatively near isotropic condition throughout the defined path. Obviously then, the 3×6 dimensionally homogenous Jacobian matrix is not suitable as a dexterity measure. Because three of the six columns of \mathbf{J}' are dependent on the other three columns, the eigenvalues of \mathbf{J}' could correspond to velocity directions in the task space which are not obtainable. Therefore, the eigenvalues and singular values of that matrix are essentially meaningless.

Figure 6 also depicts the results obtained by observing the condition number of each of the six constrained dimensionally homogeneous Jacobian matrices. Each of the constrained Jacobian matrices clearly agree that the arbitrarily chosen trajectory has the manipulator passing near a singular configuration. The six matrices $\mathbf{J}'\mathbf{P}$ are constrained based on the manipulator's motion capabilities and therefore accurately predict singular configurations,

as shown. Furthermore, their terms are dimensionally homogeneous. Therefore, their condition numbers allow a suitable means of measuring dexterity.

3.1 Reachable workspace

The reachable workspace of the 3-RRR planar parallel manipulator is depicted in Figure 7a). For the workspace plots presented in this section, the values of the architectural parameters are $r_b = 1$, $r_p = 0.4$, $b = 0.5$ and $c = 0.4$. Here, architectural parameter values are arbitrarily chosen such that results obtained in workspace analysis are comparable, in this case, with the serial RRR planar manipulator to be studied later in this chapter.

3.2 Dexterous workspace

In Section 2.3.1, six potential sets of independent end effector velocities were identified to lead to the formulation of six unique constrained and dimensionally-homogeneous Jacobian matrices. Using only one of these matrices as a dexterity measure could lead to potential bias.

To cope with having six constrained and dimensionally-homogeneous Jacobian matrices from which to measure dexterity, and the issues which arise by introducing the artificial singularity conditions discussed in Section 2.4, the minimum condition number of all six Jacobian matrices is proposed as a dexterity measure. This measure is essentially the minimum ratio between the largest actuator effort required to move in a direction in one of the six defined task-space variable sets, with the effort required to move in the easiest direction using the same task space variables. This avoids the issue of introduced singularities by the constraining matrix as the lowest condition number of the six matrices will only be high when the manipulator is near a true singular configuration.

It is also suggested that measures using the singular values also be included. By doing so, both the velocity or accuracy characteristics of the manipulator are obtained, in addition to an indication of how 'near-isotropic' the architecture is at the studied pose. In this section, the singular values of all six Jacobian matrices (provided the corresponding constraining matrix has not introduced a singularity), must lie within imposed limits.

3.2.1 Dexterity defined by the Jacobian matrix condition number

Figure 7b) depicts the dexterous workspace of the 3-RRR manipulator when the condition number of $\mathbf{J}^i \mathbf{P}_i$ (where the sub-index i refers to Case i for $i = 1 \dots 6$), is arbitrarily limited to a maximum of 60.

It can be shown that the region of the workspace removed from that of the manipulator's reachable workspace corresponds to the vicinity of a singular configuration where the three vectors \mathbf{c}_i intersect at a common point, as discussed in Section 2.4.

Figure 8 depicts the cross section of both the reachable workspace in Figure 7a) and dexterous workspace in Figure 7b) at $\phi = 0$. At this value of ϕ , the reachable workspace border at $y = 0$ and $x \approx 0.42$ corresponds to a configuration where both limbs two and three are in the fully stretched position. However, this region of the workspace also corresponds to an architectural pose near the direct singular configuration where the three vectors \mathbf{c}_i intersect. Therefore, in the vicinity of the reachable workspace border at $y = 0$, the manipulator is near both inverse and direct singular configurations. It should be expected that this region of the workspace has poor dexterity which is confirmed by Figure 8.

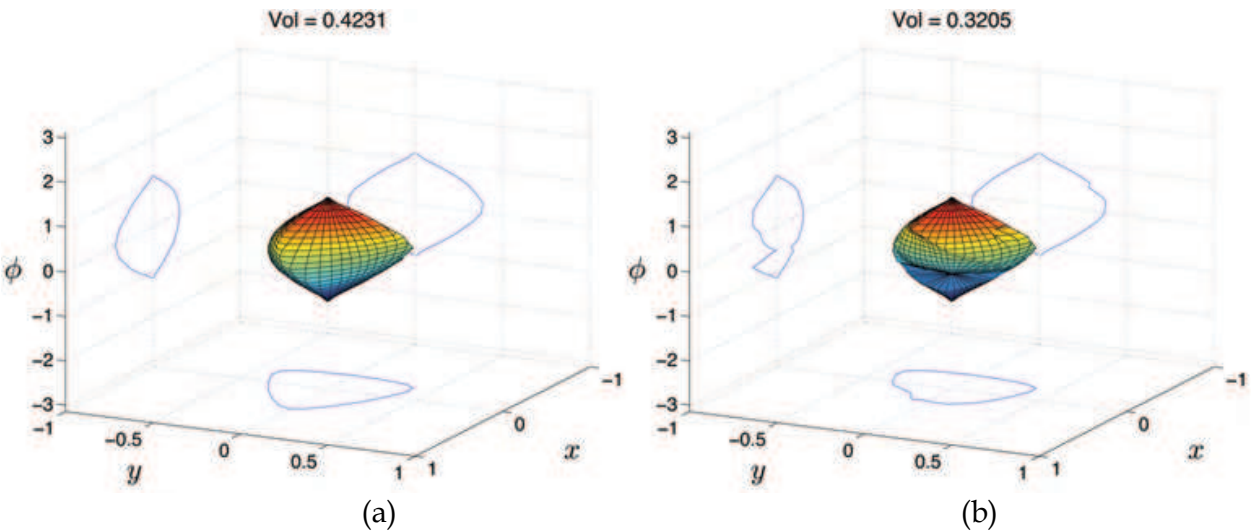


Figure 7: a) Reachable and b) dexterous workspace of the 3-RRR parallel manipulator when defined using a maximum allowable Jacobian matrix condition number of 60. Angle ϕ is expressed in radians.

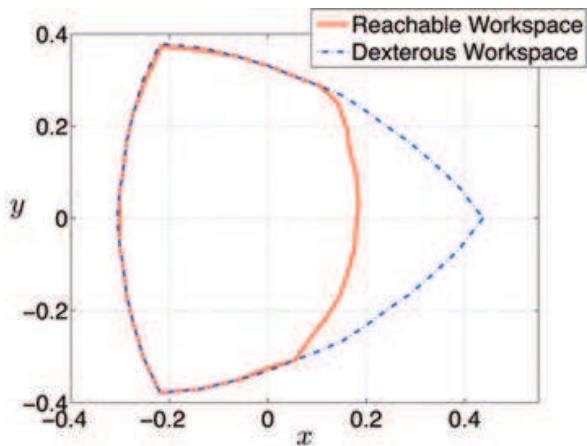


Figure 8: Cross section of both reachable and dexterous workspaces (when defined by a limit on the Jacobian matrix condition number of 60) of the 3-RRR parallel planar manipulator at $\phi = 0$.

3.2.2 Dexterity defined by the Jacobian matrix condition number and minimum singular value

The singular values within the workspace depicted in Figure 7b) vary within the range $0.0056366 \leq \sigma \leq 5.7377$. The dexterous workspace for this manipulator when also restricted to a minimum limit on the singular value of $\sigma \geq 0.1$ for any of the six Jacobian matrices is depicted in Figure 9a). An exception is made for the singular values of any of the six Jacobian matrices should that matrix falsely represent a singular configuration. The workspace in Figure 7b) has only marginally decreased in volume when compared to the dexterous workspace obtained when limiting only the Jacobian matrix condition number. The necking of the workspace at $\phi \approx -0.65$ occurs because at this pose, the manipulator is near a singular configuration where the three vectors \mathbf{c}_i intersect at a common point.

3.2.3 Dexterity defined by the Jacobian matrix condition number and maximum singular value

Similarly, a limit of $\sigma \leq 2.0$ is imposed on the six Jacobian matrices, with the exception noted earlier, to obtain the dexterous workspace for the 3-RRR manipulator depicted. The resulting workspace obtained using this upper limit is shown in Figure 9b).

Although nearly 10% greater in volume than the dexterous workspace depicted in Figure 9a), both depictions clearly indicate the same singular configuration as discussed earlier when the distal and proximal links of one of the three kinematic branches overlap.

4. The serial RRR planar manipulator

The serial RRR planar manipulator is one of the most trivial of all manipulators. For that reason, it is frequently used as a demonstration example in many texts in robot kinematics, *e.g.*, (Tsai, 1999; Craig, 2003). Through these texts, the majority of necessary work for workspace determination has been presented. Therefore only a brief summary of the required details will be presented here.

4.1 Mechanism architecture

The RRR serial planar architecture is depicted in Figure 10. It consists of three links and three actuated revolute joints. The first actuated revolute joint connects the first limb represented by vector \mathbf{b} to the base and may rotate \mathbf{b} around point O by angle θ_1 . The second actuated revolute joint at B connects the first link to the second, represented by vector \mathbf{c} . This second joint rotates \mathbf{c} with respect to \mathbf{b} by angle θ_2 . Finally, the third actuated revolute joint at C may rotate the end effector (vector \mathbf{d}) by angle θ_3 with respect to \mathbf{c} . Here, the end effector is represented as triangle $A_1A_2A_3$. Similar to the 3-RRR planar parallel architecture, the serial RRR planar architecture is confined to two translational DOF and one rotational DOF, all in the xy -plane.

4.2 Kinematics

As depicted in Figure 10, there are also two solutions to the inverse displacement problem for this manipulator. These correspond to an *elbow up* and *elbow down* configuration of the manipulator. The inverse displacement solution is provided in (Tsai, 1999; Craig, 2003).

Instead of using an alternative form of the inverse displacement solution to aid in the formulation of a dimensionally-homogeneous Jacobian matrix, it is greatly simplified in the case of serial manipulators, if the forward displacement solution is used instead. First, consider Figure 11, depicting the notation used to relate the three points on the end effector. The lengths of sides a_2 and a_3 may be found by using the cosine law:

$$\begin{aligned} a_2^2 &= r_p^2 + r_p^2 - 2r_p r_p \cos(\pi - \alpha) \\ &= 2r_p^2 - 2r_p^2 \cos(\pi - \alpha) \\ &= 2r_p^2 (1 - \cos(\pi - \alpha)) \end{aligned} \quad (31)$$

$$a_3^2 = 2r_p^2 (1 - \cos(\pi - \beta)) \quad (32)$$

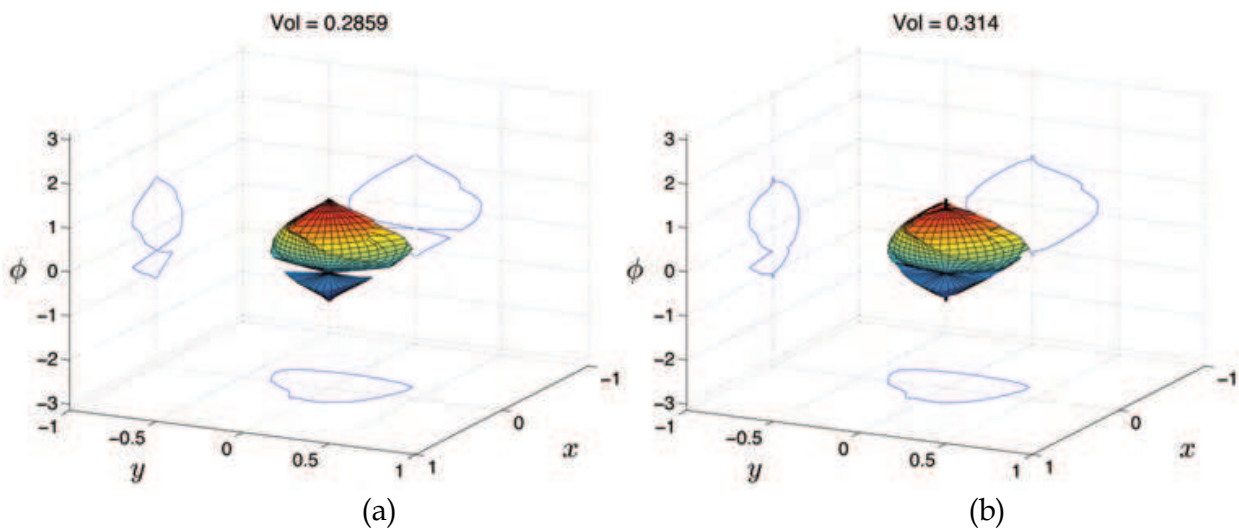


Figure 9: Dexterous workspace of the 3-RRR parallel manipulator when defined using a maximum allowable Jacobian matrix condition number and a) a minimum singular value of 0.1 or b) maximum singular value of 2. Angle ϕ is expressed in radians.

If the joint displacements were known, points B, C, A_1, A_2 and A_3 could be determined as:

$$B = \begin{bmatrix} b \cos \theta_1 \\ b \sin \theta_1 \end{bmatrix} \tag{33}$$

$$C = \begin{bmatrix} b \cos \theta_1 + c \cos(\theta_1 + \theta_2) \\ b \sin \theta_1 + c \sin(\theta_1 + \theta_2) \end{bmatrix} \tag{34}$$

$$A_1 = \begin{bmatrix} b \cos \theta_1 + c \cos(\theta_1 + \theta_2) + d \cos(\theta_1 + \theta_2 + \theta_3) \\ b \sin \theta_1 + c \sin(\theta_1 + \theta_2) + d \sin(\theta_1 + \theta_2 + \theta_3) \end{bmatrix} \tag{35}$$

$$A_2 = \begin{bmatrix} A_{1x} + a_2 \cos(\theta_1 + \theta_2 + \theta_3 + \frac{\alpha}{2}) \\ A_{1y} + a_2 \sin(\theta_1 + \theta_2 + \theta_3 + \frac{\alpha}{2}) \end{bmatrix} \tag{36}$$

$$A_3 = \begin{bmatrix} A_{1x} + a_3 \cos(\theta_1 + \theta_2 + \theta_3 - \frac{\beta}{2}) \\ A_{1y} + a_3 \sin(\theta_1 + \theta_2 + \theta_3 - \frac{\beta}{2}) \end{bmatrix} \tag{37}$$

where $\theta_1 + \theta_2 + \theta_3 = \phi$. The first derivative of these equations may be used to formulate the various elements of a dimensionally-homogeneous Jacobian matrix. As discussed in (Tsai, 1999), this manipulator is in a singular configuration whenever the manipulator is either fully extended, *i.e.*, whenever $\theta_2 = \theta_3 = 0^\circ$, or when the second link overlaps the first, *i.e.*, whenever $\theta_2 = 0^\circ$ or $\theta_2 = 180^\circ$.

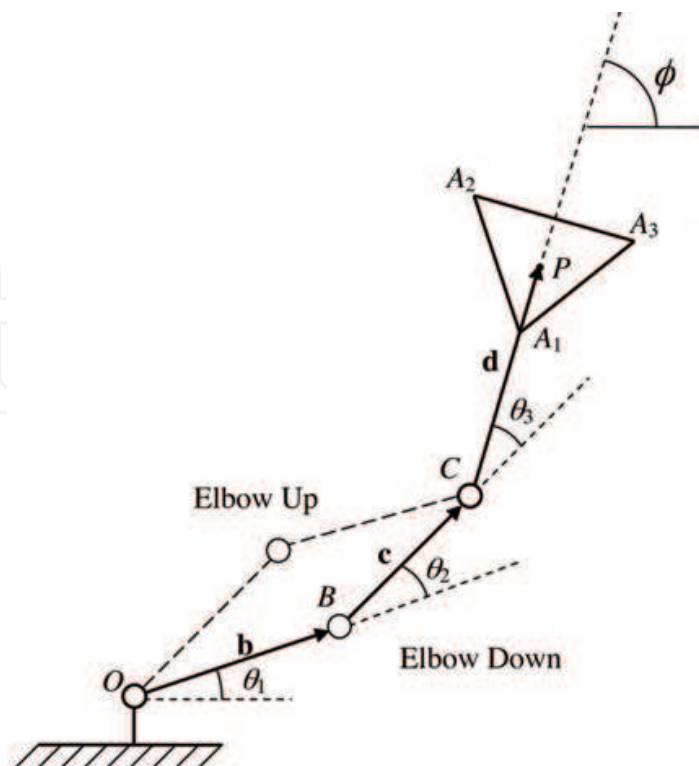


Figure 10: Architecture of the serial RRR planar manipulator.

4.3 Reachable workspace

For the serial manipulator used in the following numerical examples, architectural parameters are arbitrarily chosen to be $b = c = d = 1$. The end effector is represented as an equilateral triangle with vertices A_i . The length of each of the three line segments $\overline{A_iP}$ is equal to 1. Theoretically, infinite rotation of the end effector is obtainable in the plane; however, in order to obtain a result which may be compared to the parallel case (where for the architectural variables used, only a finite rotation was achievable), workspace envelopes obtained in the following sections will be limited to a minimum and maximum rotation of $-\pi \leq \phi \leq \pi$). The reachable workspace for this manipulator, when using the aforementioned limits, is depicted in Figure 12a). The x and y translations refer to the displacement of point P on the end effector platform depicted in Figure 10.

It is immediately clear the tremendous advantage the serial manipulator has over its parallel counterpart in terms of reachable workspace volume.

4.4 Dexterous workspace

As previously discussed, special consideration must be given to the six potential constrained and dimensionally-homogeneous Jacobian matrices that may be used to measure dexterity and the potential singularities introduced by the constraining matrix \mathbf{P}_i (for the parallel case). For the serial case, the six possible Jacobian matrices are denoted by \mathbf{J}_i corresponding to case i as noted in Section 2.3.1.

Similar to the parallel case, never will more than one of the six Jacobian matrices falsely represent a singular configuration at the same pose. However, it can be demonstrated that the condition number of all six matrices simultaneously and rapidly increase in the vicinity

of true singular configurations. Therefore, using the minimum condition number of the six Jacobian matrices remains a plausible index for dexterity.

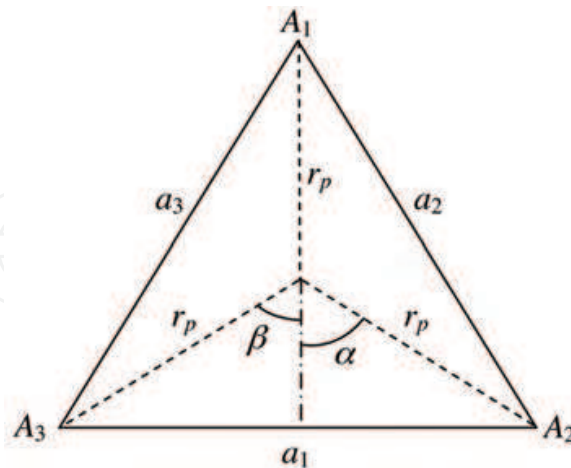


Figure 11: End effector notation for the RRR serial manipulator.

4.4.1 Dexterity measured by the Jacobian matrix condition number

Figure 12b) depicts the RRR serial manipulator's dexterous workspace when restricted to a maximum limit of 60 on the minimum condition number of any of the six Jacobian matrices (with the exception noted earlier for Jacobian matrices which falsely represent singular configurations). The portion of the workspace removed from that of the reachable workspace in Figure 12a) corresponds to the singular configuration where **b** and **c** in Figure 10 are collinear. Therefore, using a limit on the minimum Jacobian matrix condition number remains a potential index for dexterity as it is expected that the manipulator should have poor dexterity in this region. Figure 13 is a cross sectional view of the dexterous workspace depicted in Figure 12b) at $\phi = 0$. For the architectural variables used, at $\phi = 0$, the serial RRR manipulator is in an *interior* singular configuration (Tsai, 1999) at $x = 1$ and $y = 0$. At this pose, vectors **b** and **c** overlap. This is depicted in Figure 14.

4.4.2 Dexterity measured by the Jacobian matrix condition number and maximum singular value

It is important to note that the Jacobian matrix developed for the serial RRR manipulator maps $\dot{\mathbf{q}}$ to $\dot{\mathbf{x}}$ instead of $\dot{\mathbf{x}}$ to $\dot{\mathbf{q}}$ as for the 3-RRR parallel manipulator. Therefore, if a meaningful comparison is to be made, limits on the singular values of \mathbf{J}^{-1} should be imposed, rather than \mathbf{J} for the serial manipulator. This is of no consequence in the comparison of the two manipulators when the condition number limit is imposed as the condition number of \mathbf{J}^{-1} is equal to the condition number of \mathbf{J} .

The singular values of \mathbf{J}^{-1} within the workspace depicted in Figure 12b) vary within the range $0.4309 \leq \sigma \leq \infty$. It can be shown that when the singular values \mathbf{J}^{-1} are limited to $\sigma \leq 2.0$, to provide comparison to the corresponding result for the 3-RRR planar parallel manipulator, no workspace volume is obtained. Instead, for illustration purposes, Figure 15a) depicts the workspace volume where singular values are limited to $\sigma \leq 50$. Even at the relatively large allowed value for the singular values, the workspace is significantly reduced from that of Figure 12b) and is highly segmented.

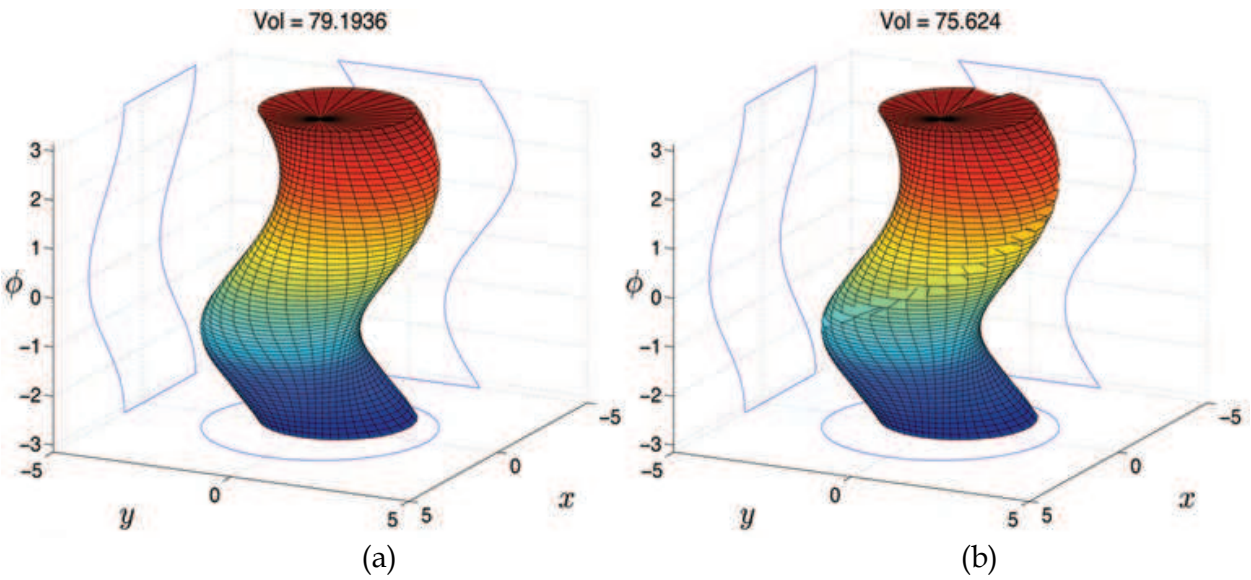


Figure 12: a) Reachable and b) dexterous workspace of the planar RRR serial manipulator when defined using a maximum allowable Jacobian matrix condition number. Angle ϕ is expressed in radians.

4.4.3 Dexterity measured by the Jacobian matrix condition number and minimum singular value

Similarly, a limit may be imposed on the minimum allowable singular value of any of the six Jacobian matrices with the exception noted earlier. When the singular values are limited to $\sigma \geq 0.1$, the dexterous workspace depicted in Figure 15b) is obtained.

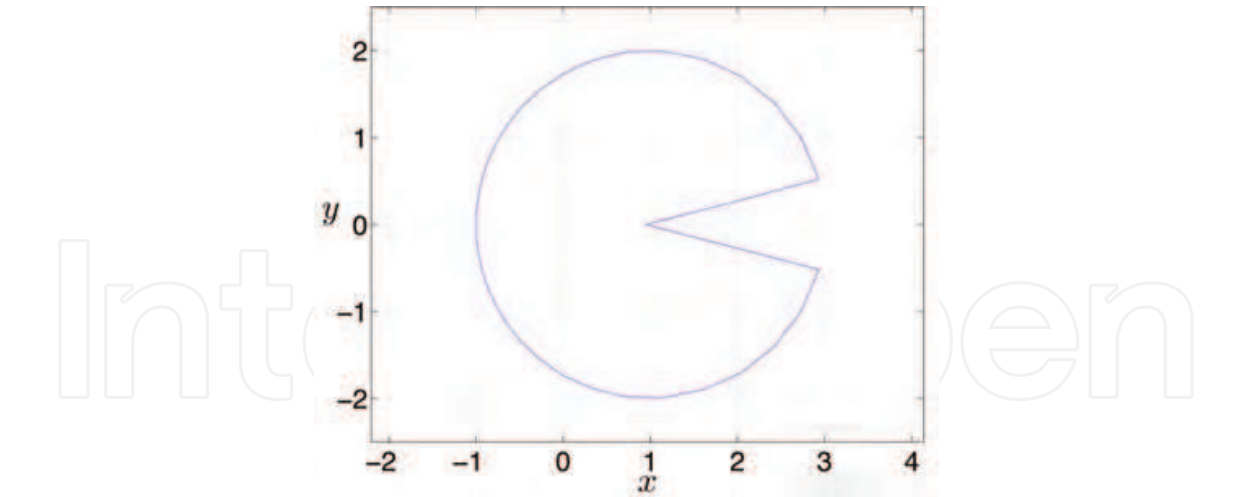


Figure 13: Cross section of the dexterous workspace when defined by a limit on the Jacobian matrix condition number of the serial RRR planar manipulator at $\phi = 0$.

Recall that the workspace corresponding to the parallel manipulator in Figure 9b) had only slightly decreased in volume when compared to that of Figure 7b). However, the workspace of the serial manipulator has not decreased at all.

Again, it should be emphasised that if architectural parameters were optimised to obtain the largest workspace volume possible, different results would be obtained.

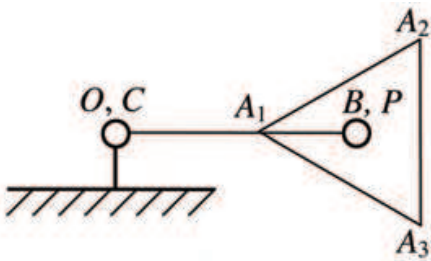


Figure 14: Singular configuration of the serial RRR manipulator.

Recall that the workspace corresponding to the parallel manipulator in Figure 9b) had only slightly decreased in volume when compared to that of Figure 7b). However, the workspace of the serial manipulator has not decreased at all. Again, it should be emphasised that if architectural parameters were optimised to obtain the largest workspace volume possible, different results would be obtained.

5. Dexterous workspace comparison of parallel and serial planar manipulators

In (Pond, 2006; Pond & Carretero, 2007), different parallel manipulators were quantitatively compared in terms of dexterity using the formulation describer earlier for the dimensionally homogeneous constrained Jacobian matrix. This section will study the effect of the arbitrarily chosen limits on the condition number and singular values on the results obtained for comparison between the serial and parallel manipulators discussed in this chapter. This is the first time such quantitative study has been made for such dissimilar architectures. For each of the following three subsections, a set of curves will be provided depicting the difference in workspace volume between the serial and parallel manipulators as the limits used to obtain them are varied. In order to better illustrate the changes, the plots are presented on suitable scales.

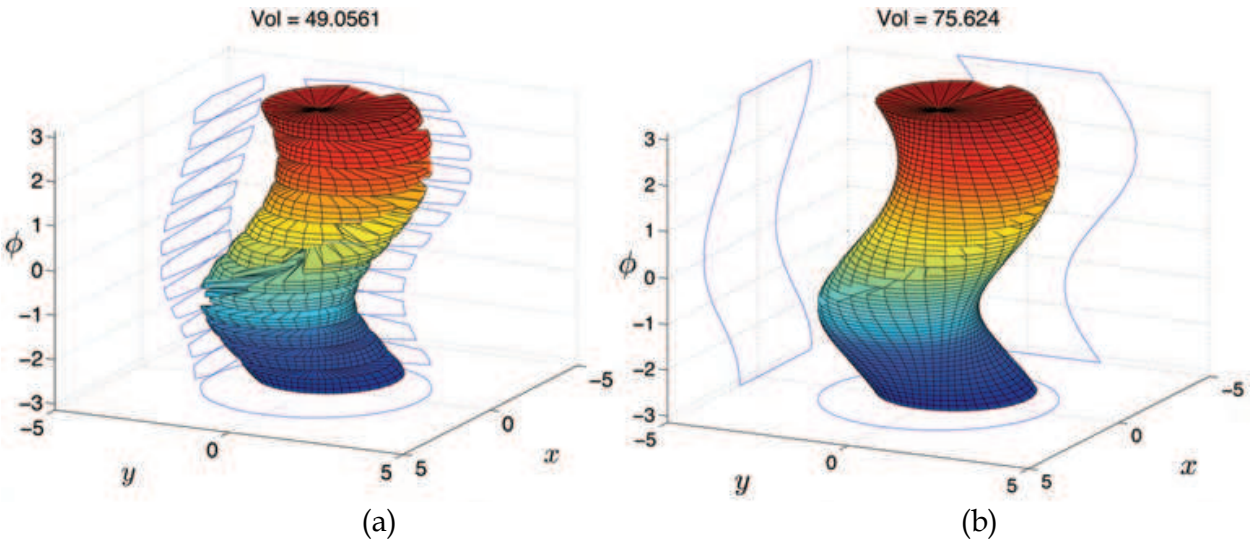


Figure 15: Dexterous workspace of the planar RRR serial manipulator when defined using a maximum allowable Jacobian matrix condition number and a) maximum singular value of 50 or b) minimum allowable singular value of 0.1. Angle ϕ is expressed in radians.

5.1 Dexterity measured by Jacobian matrix condition number

Figure 16a) depicts the dexterous workspace size as a function of the limiting value as the maximum allowable Jacobian matrix condition number. This set of curves emphasises the difference in size between the workspace of the two manipulators at limits of high condition numbers. Note that the y -axis of the graph is on a log scale.

5.2 Dexterity measured by Jacobian matrix condition number and minimum singular value

As noted earlier, the range of singular values within the serial manipulator's workspace is fairly large ($0.4309 \leq \sigma \leq \infty$). However, as Figure 16b) suggests, singular values are far denser in the lower end of this range.

In the previous section, when the singular values were limited to a minimum of $\sigma \geq 0.1$, the serial manipulator had not decreased in volume yet that of the parallel manipulator had. It is important to recall that when the limit is imposed on the lowest allowable singular value, an emphasis is being placed on obtaining high degrees of accuracy and stiffness. Figure 16b) clearly shows, however, that the volume of the serial manipulator's workspace rapidly decreases through the approximate range $0.25 \leq \sigma_{\min} \leq 0.4$. Above this range, the parallel manipulator provides the largest workspace volume.

Therefore, these results suggest that, of the two manipulators, for the architectural variables used, the parallel manipulator outperforms the serial manipulator within the range of approximately $\sigma_{\min} \geq 0.4$. Naturally, this conclusion can only be made for the specific architectural variables used in this study.

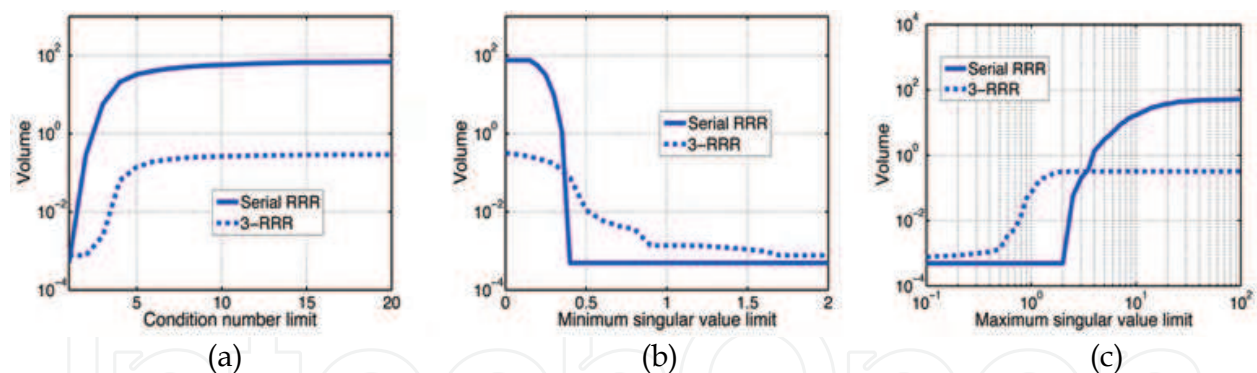


Figure 16: Dexterous workspace comparison based on a) a limit on the condition number, b) a limitation on the minimum allowable singular value, and c) a limitation on the maximum allowable singular value.

5.3 Dexterity measured by Jacobian matrix condition number and maximum singular value

Figure 16c) compares the dexterous workspace volumes of both the serial and parallel planar manipulators when limited by the condition number and a maximum singular value. Recall that the range of singular values within the serial manipulator's workspace is much larger than the corresponding range for the parallel manipulator. The workspace volume of the serial manipulator only begins to significantly increase in volume at a relatively higher

limit of approximately $\sigma_{\max} \geq 2$. Conversely, at this limit, the workspace corresponding to the parallel manipulator has obtained its full volume as depicted in Figure 16c).

This is an interesting result as lower singular values correspond to higher end effector velocities. This suggests that the parallel architecture studied also provides the largest workspace volume when high end effector velocities are required, to a limit of approximately $\sigma_{\max} \geq 4$ where the serial manipulator then provides the largest workspace volume.

6. Conclusions

Through either method of obtaining a constrained dimensionally homogeneous Jacobian matrix (proposed by (Gosselin, 1992) or by (Pond & Carretero, 2006)) for planar mechanisms, a choice exists on which of the potential six Cartesian velocity components on the end effector be used to define the task space velocity variables. The choice has an influence on the resulting Jacobian matrix and therefore its condition number and singular values. Without constraining the Jacobian matrix, the condition number was demonstrated to be essentially meaningless, as in (Kim & Ryu, 2003).

In terms of measuring dexterity, the constrained dimensionally homogeneous Jacobian matrices ($\mathbf{J}^{\mathbf{P}}$) are superior to the screw based Jacobian matrix (\mathbf{J}) in that they are dimensionally consistent. Furthermore, the six matrices ($\mathbf{J}^{\mathbf{P}}$) are superior to the 3×6 dimensionally homogeneous matrix (\mathbf{J}) in that they are constrained, and therefore provide true dexterous information.

The condition number and singular values of each of the six matrices ($\mathbf{J}^{\mathbf{P}}$) are different for any given pose. Therefore, dexterity measures involving only one of the six ($\mathbf{J}^{\mathbf{P}}$) matrices are potentially bias. Four potential strategies for dexterity measurement have been proposed based on the condition number and/or singular values of the Jacobian matrices obtained in all six cases. Each measure has a distinct physical meaning, as discussed.

In sum, the Jacobian matrix formulation presented in this chapter allows, for the first time, to *quantitatively* compare different mechanism architectures with complex degrees of freedom in terms of dexterity. Moreover, as illustrated in this chapter, the formulation is not limited to parallel manipulators as it can also be used to quantitatively compare the dexterity of different architectures as long as the end effector is represented by an equivalent set of points. Quantitative dexterity comparisons will allow robot designers to better select proper mechanisms for specific tasks.

7. References

- J. Angeles (2003). *Fundamentals of Robotic Mechanical Systems*, Springer-Verlag, ISBN: 978-0-387-95368-7, New York.
- M. Arsenault & R. Boudreau (2004). The synthesis of three-degree-of-freedom planar parallel manipulators with revolute joints (3-RRR) for an optimal singularity-free workspace. *Journal of Robotic Systems*, Vol.21, No.5, page numbers (259-274).
- M. Badescu & C. Mavroidis (2004). Workspace optimization of 3-legged UPU and UPS parallel platforms with joint constraints. *Journal of Mechanical Design*, Vol.126, No.2, page numbers (291-300), ISSN: 1050-0472.

- I. A. Bonev & C. M. Gosselin (2001). Singularity loci of planar manipulators, Proceedings of the 2nd workshop on computational kinematics, Seoul, South Korea, 2001.
- J. A. Carretero; R. P. Podhorodeski; M. A. Nahon & C. M. Gosselin (2000). Kinematic analysis and optimization of a new three degree-of-freedom spatial parallel manipulator. *Journal of Mechanical Design*, Vol.122, No.1, page numbers (17-24), ISSN: 1050-0472.
- J. J. Craig (2003). *Introduction to Robotics: Mechanics and Control*, Prentice Hall, ISBN: 978-0-201-54361-2, New York.
- K. L. Doty; C. Melchiorri; E. M. Schwartz & C. Bonivento (1995). Robot manipulability. *IEEE Transactions on Robotics and Automation*, Vol.11, No.3, page numbers (462-268), ISSN: 1042-296X.
- C. M. Gosselin (1988). *Kinematic analysis, optimization and programming of parallel robotic manipulators*, Ph.D thesis, Department of Mechanical Engineering, McGill University, ISBN: 0315485043, Montreal, Canada.
- C. M. Gosselin & J. Angeles (1989). The optimum kinematic design of a spherical three-degreeof- freedom parallel manipulator. *Journal of Mechanisms, Transmissions, and Automation in Design*, Vol.19, No.4, page numbers (202-207), ISSN: 0738-0666.
- C. M. Gosselin (1992). The optimum design of robotic manipulators using dexterity indices. *Journal of Robotics and Autonomous Systems*, Vol.9, No.4, page numbers (213-226).
- S. G. Kim & J. Ryu (2003). New dimensionally homogeneous Jacobian matrix formulation by three end-effector points for optimal design of parallel manipulators. *IEEE Transactions on Robotics and Automation*, Vol.19, No.4, page numbers (731-737), ISSN: 1042-296X.
- K. Lee & D. Shah (1988). Kinematic analysis of a three-degree-of-freedom in parallel actuated manipulator. *IEEE Journal of Robotics and Automation*, Vol.4, No.3, page numbers (354- 360), ISSN: 0882-4967.
- G. Pond (2006). *Dexterity and workspace characteristics of complex degree of freedom parallel manipulators*, Ph.D thesis, Department of Mechanical Engineering, University of New Brunswick, Fredericton, Canada.
- G. Pond & J. A. Carretero (2006). Formulating Jacobian matrices for the dexterity analysis of parallel manipulators. *Mechanism and Machine Theory*, Vol.41, No.12, page numbers (1505-1519), ISSN: 0094-114X
- G. Pond & J. A. Carretero (2007). Quantitative dexterous workspace comparisons of parallel manipulators. *Mechanism and Machine Theory*, Vol.42, No.10, page numbers (1388-1400), ISSN: 0094-114X.
- B. Siciliano (1999). The Tricept robot: inverse kinematics, manipulability analysis and closedloop direct kinematics algorithm. *Robotica*, Vol.17, No.4, page numbers (437-445), ISSN: 0263-5747.
- D. Stewart (1965). A platform with six degrees of freedom, Proceedings of the Institute of Mechanical Engineering, pp. 371-386, London, UK, 1965.
- G. Strang. (2003). *Introduction to Linear Algebra*, Wellesley Cambridge Pr, ISBN: 978-0-961-40889-3, Wellesley MA.
- L.-W. Tsai. (1999). *Robot Analysis: The Mechanics of Serial and Parallel Manipulators*, John Wiley and Sons Inc., ISBN: 978-0-471-32593-2, New York.

L.-W. Tsai & S. Joshi (2000). Kinematics and optimization of a spatial 3-UPU parallel manipulator. *Journal of Mechanical Design*, Vol.122, No.4, page numbers (439-446), ISSN: 1050-0472.

IntechOpen

IntechOpen



Parallel Manipulators, New Developments

Edited by Jee-Hwan Ryu

ISBN 978-3-902613-20-2

Hard cover, 498 pages

Publisher I-Tech Education and Publishing

Published online 01, April, 2008

Published in print edition April, 2008

Parallel manipulators are characterized as having closed-loop kinematic chains. Compared to serial manipulators, which have open-ended structure, parallel manipulators have many advantages in terms of accuracy, rigidity and ability to manipulate heavy loads. Therefore, they have been getting many attentions in astronomy to flight simulators and especially in machine-tool industries. The aim of this book is to provide an overview of the state-of-art, to present new ideas, original results and practical experiences in parallel manipulators. This book mainly introduces advanced kinematic and dynamic analysis methods and cutting edge control technologies for parallel manipulators. Even though this book only contains several samples of research activities on parallel manipulators, I believe this book can give an idea to the reader about what has been done in the field recently, and what kind of open problems are in this area.

How to reference

In order to correctly reference this scholarly work, feel free to copy and paste the following:

Geoff T. Pond and Juan A. Carretero (2008). Quantitative Dexterous Workspace Comparison of Serial and Parallel Planar Mechanisms, Parallel Manipulators, New Developments, Jee-Hwan Ryu (Ed.), ISBN: 978-3-902613-20-2, InTech, Available from:

http://www.intechopen.com/books/parallel_manipulators_new_developments/quantitative_dexterous_workspace_comparison_of_serial_and_parallel_planar_mechanisms

INTECH
open science | open minds

InTech Europe

University Campus STeP Ri
Slavka Krautzeka 83/A
51000 Rijeka, Croatia
Phone: +385 (51) 770 447
Fax: +385 (51) 686 166
www.intechopen.com

InTech China

Unit 405, Office Block, Hotel Equatorial Shanghai
No.65, Yan An Road (West), Shanghai, 200040, China
中国上海市延安西路65号上海国际贵都大饭店办公楼405单元
Phone: +86-21-62489820
Fax: +86-21-62489821

© 2008 The Author(s). Licensee IntechOpen. This chapter is distributed under the terms of the [Creative Commons Attribution-NonCommercial-ShareAlike-3.0 License](https://creativecommons.org/licenses/by-nc-sa/3.0/), which permits use, distribution and reproduction for non-commercial purposes, provided the original is properly cited and derivative works building on this content are distributed under the same license.

IntechOpen

IntechOpen